Precision Agric
DOI 10.1007/s11119-016-9479-0

# Investigation and analysis of an ultrasonic sensor for specific yield assessment and greenhouse features identification

**R. Finkelshtain[1,3] · A. Bechar[1] · Y. Yovel[2] · G. Kósa[3]**



**Abstract** The spectrum of an ultrasonic return echo from plants has been shown to contain useful information. The research reported in this paper focused on developing an ultrasonic sensing system and analyzing the ultrasonic classification features that would ultimately be used as the basis for a yield estimation robotic system. An algorithm was also developed for prediction of fruit mass per plant based on the ultrasonic echo return from a plant. The ultrasonic sensor system was tested in lab and pepper greenhouse environments and on single pepper plants, single leaves and fruit. The results showed the potential of ultrasonic sensors for such a robot in classifying plants and greenhouse infrastructures such as walls. It showed the robot's ability to detect hidden plant rows and fruits as well as making an estimation of the fruit mass in single plants. A multi-linear regression model developed for estimating the energy level was found to be highly significant with $R^2$ of 0.64 and 0.84 for 28–32 and 20–28 kHz ranges respectively. This estimated model was used to derive a prediction method for fruit mass per plant that yielded an $R^2$ of 0.34.

**Keywords** Plant recognition · Ultrasonic sensing · Yield assessment · Sonar

## Introduction

Specific yield assessment is essential for precision farming. In addition, it is an important tool in agriculture for planning crop revenues, budget, store capacity, labour management and compensation calculations. In several crops, such as deciduous trees, fruit thinning is

✉ R. Finkelshtain
roeefink@mail.tau.ac.il

[1] Institute of Agricultural Engineering, Agricultural Research Organization (ARO), Rishon LeZion, Israel

[2] Faculty of Life Sciences, Tel Aviv University (TAU), Tel Aviv, Israel

[3] School of Mechanical Engineering, TAU, Tel Aviv, Israel

Published online: 17 November 2016

done based on the yield estimation. However, the present techniques for yield assessment are labour intensive and hence tend to be expensive. Moreover, the process is inaccurate as it is carried out manually by workers in the field and is based on crop sampling in small quantities and therefore, in addition, loses the variation information. There is a tradeoff between the amount of time invested in sampling the crop and the accuracy given the inhomogeneous nature of crop distribution. To meet this challenge, various modern sensing technologies, such as thermal imaging (Stajnko et al. 2004), depth cameras (Andújar et al. 2015) and optical methods (Wachs et al. 2010) have been suggested for development of an automated system for detection of crop biomass and yield estimation (Lee et al. 2010).

Vision-based crop estimation has been used in the context of specialty crops. Moonrinta et al. (2010) developed a vision-based pineapple mapping algorithm with a detection success rate of 80%. Another vision-based yield estimation that was described by Nuske et al. (2011) managed to detect 50–70% of the visible grapefruit and predicted the amount of crop mass with an error of 9%.

Ultrasonic sensing is a non-contact sensing technology that acquires information by transmitting high frequency sounds at objects and recording and analyzing the echo returns from them (Kleeman and Kuc 2008). The aforementioned authors also note that as the time it takes for sound waves to propagate is proportional to distance, ultrasonic sensors are popular mainly as proximity sensors. Another use for ultrasonic sensors is for object classification. Akbarally and Kleeman (1995) used ultrasonic sensing for indoor geometrically-based classification and location of walls and edges, by analyzing the time of flight from two or three receivers. Lim et al. (2012) improved this method by adding more receivers and developing a statistical measure for classification.

The absorption of energy is dependent upon the frequency, geometry, texture and acoustic impedance of the reflectors. Based on these facts, an alternate, bio-mimetic approach was used for ultrasonic classification: analyzing the spectral content of the echo. Steckel and Peremans (2013) translated positions in an indoor environment to ultrasonic features and discriminated between them using an advanced neural network for indoor simultaneous location and mapping (SLAM). McKerrow and Harper (1999) presented a way to extract geometric features of plants from the returned echo using a machine perception method to differentiate between different plants. Müller and Kuc (2000) studied bat sonar by analyzing the returns from foliage and extracting high confidence level statistically invariant features from them. Yovel et al. (2008) managed to classify four different species of plants by their echoes by using a machine learning algorithm. Yovel et al. (2009) found repeating patterns that link between the echoes and plants. Based on these patterns, they derived statistical models and created artificial plants that, when compared to the signals of real plants, gave high fit ratios. Balleri et al. (2012) have discriminated between pollinated and non-pollinated flowers of the *Mucuna holtonii* plant which has nectar that is fancied by bats.

The literature on object classification in agriculture using ultrasonic sensing is limited. Most studies in agriculture deal with evaluation of physical and biological properties of fruits and vegetable (Mizrach et al. 2003; Mizrach 2008). Andújar et al. (2011) presented a method for identifying one of three different possible plants: broad leaved weeds, grasses and their mixture by using spectrum-based classification. Toda et al. (1999) created a fuzzy logic navigation algorithm that worked in maize rows organized in a lab to simulate a field. Harper and McKerrow (2001) suggested an algorithm for mobile robot navigation by using plants as landmarks.

The advantages of ultrasonic sensing for yield assessment are threefold: sound waves are capable of propagating through the foliage and can detect hidden fruit while other

sensors require a direct line of sight; transmission of a wide frequency multi-spectral acoustic signal range (20–200 kHz) enables classification of plant properties; high-resolution distance measurement enables a reliable spatial dimension for discriminating parts of the plant through the analysis and estimation stages.

The objectives of the research were: characterization of useful information from the plant acoustic spectrum and its classification in real time to make a robotic ultrasonic system for yield assessment.

## Materials and methods

### Definitions

The following re-occurring terms are important for the understanding of this study:

*Compressed High Intensity Radar Pulse* (*CHIRP*) A signal with a varying frequency over time. Despite the word "radar" in the acronym the term is commonly used in the field of ultrasonic sensing (also referred to as frequency modulated signals and sweep signals).

*Ensonify* To fill with sound.

*Spectrogram* Representation of a signal intensity in the time–frequency space.

*Frequency response* Representation of the signal intensity in the frequency domain. The frequency response is defined in this paper as the sum of the echo amplitudes in a specific frequency divided by the mean CHIRP amplitude of the same frequency.

### Instrumentation

The experimental system comprised of two parts: an ultrasonic sensing system and an RGB camera. The main components of the ultrasonic sensing system were a loudspeaker and a microphone, (1) and (2) in Fig. 1 respectively. The speaker (XT25SC90-04, Tymphany,

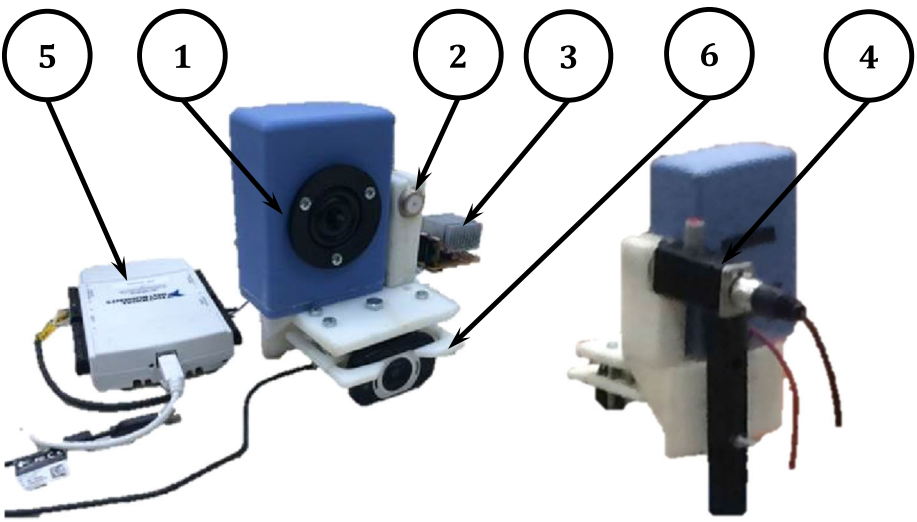


**Fig. 1** Front and back view of the sensing system that has: *1* Ultrasonic loudspeaker, *2* Ultrasonic Microphone, *3* Loudspeaker amplifier, *4* Microphone supply and amplifier, *5* DAQ card and *6* Camera

Sausalito, CA, USA) has a highly flat frequency response specified as 1–40 kHz and as far as 120 kHz in practice. The ultrasonic microphone is electro-static (CM16/CMP, Avisoft Bioacoustics, Glienicke, Germany) and has a flat frequency response in the range of 10–150 kHz with a sensitivity of 50 $mVPa^{-1}$. The signal to the ultrasonic loudspeaker was from a custom op-amp amplifier (PA12, Apex Microtechnology, Tucson, AR, USA), (3) in Fig. 1, with a gain of 2–7 and bandwidth of 160 kHz. The microphone had an adjustable amplifier and power supply (CMPA40-5V, Avisoft Bioacoustics, Glienicke, Germany), (4) in Fig. 1, supplying 200 V polarization voltage. The output to the loudspeaker and the input from the microphone was processed by a data acquisition (DAQ) device (USB-6210, National Instruments, Austin, TX, USA), (5) in Fig. 1, with 16 Bit resolution at a sampling frequency of 250 kHz (analog input and output sample rate). The RGB camera was used for comparison to the ultrasonic data. The HD Webcam C615 (Logitech, Lausanne, Switzerland) worked at 640 × 480 resolution in trigger mode.

## Data acquisition and basic signal processing

A first step in multi-spectral analysis of ultrasonic recordings was to acquire the ensonified object's impulse response. Emitting a pure Dirac delta style impulse signal with a loudspeaker is not possible. Müller and Massarani (2001) suggested that, for characterizing of a room's acoustic parameters, CHIRPs are the favored signal type in terms of signal to noise ratio (SNR).

The frequency response was derived by transmitting an ultrasonic linear CHIRP (marked by a solid rectangle in Fig. 2b) at objects and comparing it to the attenuated return echo (marked by a dashed rectangle). The ensonification was recorded (Fig. 2a) and transformed into a spectrogram using the short time Fourier transform algorithm with a rectangular window of 100 time-steps, a 50 time-step overlap between windows and 256 frequency bins (Fig. 2b). The time axis was transformed according to the frequencies' ensonification time so that the spectrogram's horizontal axis would represent distance from the sensor (Fig. 2c).

The CHIRP and echo spectrograms were extracted separately from the spectrogram and were analyzed by operating over the frequency or distance dimensions using statistical, image processing or signal processing techniques. The frequency response was defined in

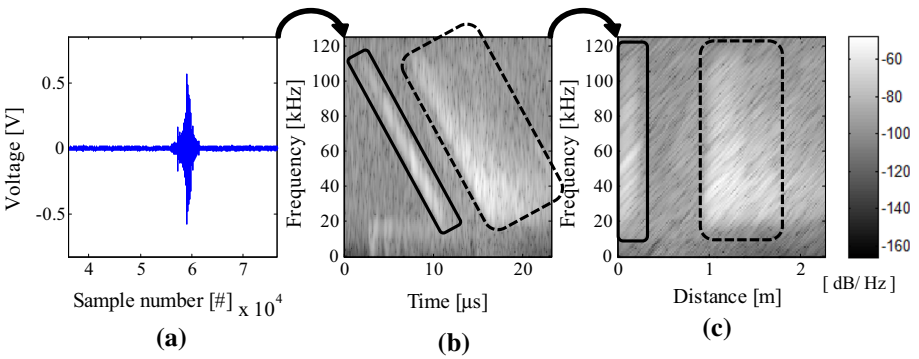


**Fig. 2** Basic data processing steps: **a** Recorded signal. **b** Frequency–time spectogram. **c** Frequency–distance spectogram

this study as the sum of the echo amplitudes at a specific frequency normalized by the mean CHIRP amplitude at the same frequency.

## Experiments

Three experiments were conducted and are shown in Fig. 3: (i) A greenhouse classification experiment using the ultrasonic sensor to obtain a wide variety of ultrasonic echoes of plants, crop rows, common objects and infrastructures. (ii) A single fruit and leaf experiment to determine the frequency response of single leaves and fruit—the basic building blocks of the full plant echoes; and, (iii) A lab experiment, in which the influence of fruit mass on the frequency response of different plants from different orientations and different distances was measured focused in the quantitative estimation of fruit yield based on statistical analyses of the ultrasonic echoes.

### *Greenhouse classification experiment*

The experiment was conducted in the research greenhouse of the agricultural robotics lab (ARL) at the agricultural research organization (ARO). The ultrasonic recordings were taken in different combinations of (i) distances (ii) number of crop rows between the object and the ultrasonic sensor, and (iii) object type. The experimental system was set in the following configurations: (1) Sensing system was perpendicular to an empty place in the greenhouse with no crop rows (measures the return echoes from the ground); (2) Sensing system was perpendicular to three successive pepper crop garden beds; (3) Sensing system was perpendicular to the greenhouse plastic wall; and, (4) Sensing system is perpendicular to two cucumber rows. The distances from the target in these experiments are summarized in Table 1.

A linear CHIRP ranging 20–120 kHz in 10 ms was selected as the excitation signal. The transmitting amplitude was set to minimize saturation by changing the speaker and microphone amplifier gains. The object picture, ultrasonic echoes and distance were taken at least 30 times for each configuration.


**Fig. 3** Experimental setups **a** Greenhouse classification experiment. **b** Single fruit and leaves experiment. **c** Laboratory experiment

**Table 1** Distance configurations

| Distances (m) | Exp. 2 | Exp. 3 | Exp. 4 |
|---|---|---|---|
| 0.5 | √ | √ | – |
| 1 | √ | √ | √ |
| 1.5 | √ | √ | √ |
| 2 | √ | √ | – |

*Single fruit and leaf experiment*

The experiment was conducted indoors at the Robots and BioMedical Micro Systems lab at Tel-Aviv University (TAU). Five different freshly picked leaves and fruit were ensonified 50 times by linear CHIRP excitations ranging 5–120 kHz in 5 ms time. The distance to the ensonified objects was 1 m and the orientations of the objects were randomly changed. In order to isolate their echoes, the fruit and leaves were ensured to be the only objects in the vicinity of the sensing system by tying them to the ceiling by a thin thread. The thread was ensonified and confirmed to return weak echoes below the sensing system detecting threshold.

*Lab experiment*

This experiment took place in the ARL. Five fully grown pepper plant samples (Fig. 3c) with a total fruit mass of 700–1200 g per plant were carefully uprooted from the ARL research greenhouse and planted in pots. The plants were held by thin threads hanging from the ceiling to replace the trellising while minimizing any noise to the return echoes caused by anything other than the plants. The five plants were ensonified with a 20–120 kHz in 5 ms linear CHIRP for 30 times from three orientations, 120° apart—denoted as plant #*i* orientation #*j* ($P_iO_j$). Each $P_iO_j$ was ensonified from distances of 0.625 and 1.25 m and for three fruit levels. A multi-linear regression and a fruit mass estimation method were conducted based on the experiment results was conducted in post processing.

## Attenuation and hidden row detection

Most of the energy returned from a plant was concentrated in proximity of the main stem where the density of leaves that act as the main sound reflectors is high (Yovel et al. 2009). The mean spectrograms of the stem area generally showed that higher frequency sounds were more strongly attenuated. Ping (1998) suggested that the attenuation of sound can be described as an exponential function of the frequency and distance. The sound pressure decays exponentially according to Eq. (1) where $\alpha(f)$ is the attenuation at frequency $f$, $x$ is the distance and $E_N^{ij}(x,f)$ is the energy compensated for attenuation.

$$E^{ij}(x,f) = E^{ij}(0,f)e^{-\alpha(f)x} \rightarrow E_N^{ij}(x,f) = \frac{E^{ij}(x,f)}{e^{-\alpha(f)x}} \tag{1}$$

The attenuation for each frequency was derived using ordinary least squares (OLS) on the frequency response results of the greenhouse classification experiment. The attenuation was used to normalize the energy returning from a row by using the attenuation values as weights to compensate for the energy loss due to distance. However, it amplifies the noise too. To overcome that, the noise was filtered prior to amplification. The return energies of

the plants were relatively strong in the 40–60 kHz band, therefore the detection process was done in that frequency band. Finally, the cross correlation of the CHIRP with the compensated return echo (also known as a matched filter) was used to maximize the SNR and to detect the plant rows by thresholding.

## Statistical analysis

The sum of energy of a plant echo per frequency bin contained information that was assumed to be unbiased by fruit distance to the sensing system as the fruits were distributed normally (Bloch et al. 2015). This individual frequency bin sum of energy returned from $P_iO_j$ is denoted as $E^{ij}$. To examine the hypothesis that $E^{ij}$ was a monotonic function of the fruit mass, $m^{ij}$ and influenced by the ensonified frequency, $f^{ij}$, a multiple linear regression model was defined. The actual physical relationships between the listed factors expressed as $E^{ij} = F(m^{ij}, f^{ij}, x^{ij})$, was theoretically intractable, where $x^{ij}$ is unknown and represents specific factors of $P_iO_j$ that are unobserved since the geometry of a pepper plant was complex and specific for each specimen. However, given that $F(m^{ij}, f^{ij}, x^{ij})$ was $n$-order differentiable, the Taylor theorem could be applied to establish a $n$-ordered polynomial approximation to the above relationships and estimate its parameters as a regression model. Equation (2) shows the second order approximation of $F(m^{ij}, f^{ij}, x^{ij})$ around $\bar{m}, \bar{f}$, the mean mass and mean frequency respectively. For compactness reasons, $F(\bar{m}, \bar{f}, x^{ij})$ and its derivatives are marked $\bar{F}, \bar{F}_m, \bar{F}_f, \bar{F}_{mf}, \bar{F}_{mm}, \bar{F}_{ff}$.

$$E^{ij} \cong \bar{F} + (m^{ij} - \bar{m})\bar{F}_m + (f^{ij} - \bar{f})\bar{F}_f + (m^{ij} - \bar{m})^2\bar{F}_{mm} + (f^{ij} - \bar{f})^2\bar{F}_{ff} + 2(m^{ij} - \bar{m})(f^{ij} - \bar{f})\bar{F}_{mf} \tag{2}$$

Assuming that the second order approximation is satisfying, Eq. (2) leads to a linear regression model (Eq. 3):

$$E^{ij} = \alpha + \alpha_{11}\delta^{11} + \alpha_{12}\delta^{12} + \cdots + \alpha_{53}\delta^{53} + \beta_m m^{ij} + \beta_f f^{ij} + \gamma_{mm} m^{ij2} + \gamma_{ff} f^{ij2} + \gamma_{fm} m^{ij} f^{ij} + \varepsilon^{ij} \tag{3}$$

Assuming $\varepsilon^{ij}$ is the model random and serially uncorrelated error, the model parameters denoted by $\alpha, \beta, \gamma$ are computed via OLS. $\delta^{ij}$ are indicator variables defined in Eq. (4) and are assigned to address and quantify the fixed influence of $x^{ij}$.

$$\delta^{ij} = \begin{cases} 1 & \text{if plant i orientation j} \\ 0 & \text{otherwise} \end{cases} \tag{4}$$

By solving the quadratic Eq. 3 for the mass term, an estimation of fruit mass depending on the specific specimen terms $\alpha_{ij}\delta^{ij}$ can be derived (Eq. 5). As $\alpha_{ij}\delta^{ij}$ is unknown for new plants, the estimation function in its present form is of little use.

$$0 \cong \underbrace{\gamma_{mm}}_{a} m^{ij2} + \underbrace{\left(\beta_m + \gamma_{fm} f^{ij}\right)}_{b} m^{ij} + \underbrace{\alpha + \alpha_{11}\delta^{11} + \alpha_{12}\delta^{12} + \cdots + \alpha_{53}\delta^{53} + \beta_f f^{ij} + \gamma_{ff} f^{ij2} + E^{ij}}_{c}$$

$$\overset{yields}{\rightarrow} m^{ij} = \frac{-b \pm \sqrt{b^2 - 4ac}}{2a} \tag{5}$$

The derivative of $F(m^{ij}, f^{ij}, x^{ij})$ in respect to the frequency and mass is of special interest. The indicator variables cancel out by differentiating with respect to $f^{ij}$ which allows the isolation of an expression for mass using the regression model parameters as in Eq. (6). This comes with a cost of noisy numerical differentiation but it allows the prediction of fruit mass with the measured energy $E^{ij}$ regardless of the unknown specific specimen factors, $x^{ij}$.

$$\frac{\partial E^{ij}}{\partial f^{ij}} = \beta_f + 2\gamma_{ff} f^{ij} + \gamma_{fm} m^{ij} \overset{\text{yields}}{\rightarrow} m^{ij} = \frac{\frac{\partial E^{ij}}{\partial f^{ij}} - \beta_f - 2\gamma_{ff} f^{ij}}{\gamma_{fm}} \tag{6}$$

## Results

### Greenhouse features characterization

#### *Ground reflections*

The sensing system was mounted perpendicular to an empty area in the greenhouse with no crop rows (Fig. 4a) and measured the return echoes from the ground. Figure 4b shows the ground mean echo of 30 spectrograms from this position. The spectrogram indicated that there were substantial energy returns from a distance of 0.72 m up to 2.2 m away from the sensing system. At this range, the echo was high for frequencies between 20 and 60 kHz.

The source of these returns could be only the ground, which is in compliance with the cone shaped main lobe broadcasting characteristics of the speaker. Therefore, the ground signature should be considered in any implementation of the sensor system. The ground echo can be filtered from the spectrogram assuming that the sensing system remains at the same height.

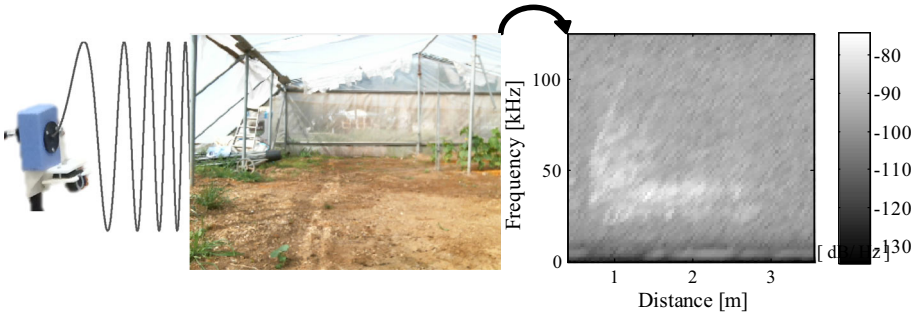


**Fig. 4** **a** View from the sensor of an empty space in the greenhouse. **b** Ground mean spectrogram

*Detection of crop rows*

Figure 5a shows two parallel pepper garden beds, each garden bed had two pepper rows. The mean echo spectrogram of the ensonifications taken from a distance of 0.5 m from the first row is shown in Fig. 5b, with the correlation sum at 40–60 kHz representing the echo strength for each distance from the sensor. The correlation sum was calculated according to the methodology presented in the "Attenuation and hidden row detection" section above. The four peaks in the correlation sum curve in Fig. 5b represent the four plant rows (separated into two garden beds) and are detectable by either thresholding or searching the local maxima of the plot. The ability to detect and determine the distance to objects occluded by foliage (the second pepper garden bed) in the greenhouse environment is a unique feature of spectrum-based ultrasonic sensing.

*Greenhouse wall and vegetation*

The sensing system was mounted at a distance of 1.0 m perpendicular to the greenhouse plastic wall and to a pepper plant row. Figure 6 illustrates the mean frequency response obtained from these samples. The differences between plant and wall is expressed at frequencies between 70 and 105 kHz. Furthermore, the echo duration of the wall was shorter and stronger than that of the plants due to depth and porosity of the objects. A set of such wall and plant frequency response vectors was used to train a support vector machine to classify between them (Finkelshtain et al. 2015).

## Single fruit experiment

The mean frequency spectrum of a single leaf and fruit at random orientations is presented in Fig. 7. The results indicate that the spectrum of a single leaf and fruit were similar at all frequencies except for two peaks and their neighborhood frequencies at 33 kHz in which the single leaves had higher intensities and the opposite at 70 kHz.

McKerrow and Kristiansen (2006) developed a theoretical model explaining the echo returns from rough surfaces based on the assumption that the energy returns to the transmitting origin only from surfaces nearly perpendicular to the sensor system. This explains the behavior of the single leaf spectrum as their shape is approximately flat and return more energy as apparent from Fig. 7 at 33–55 kHz. The single fruit second

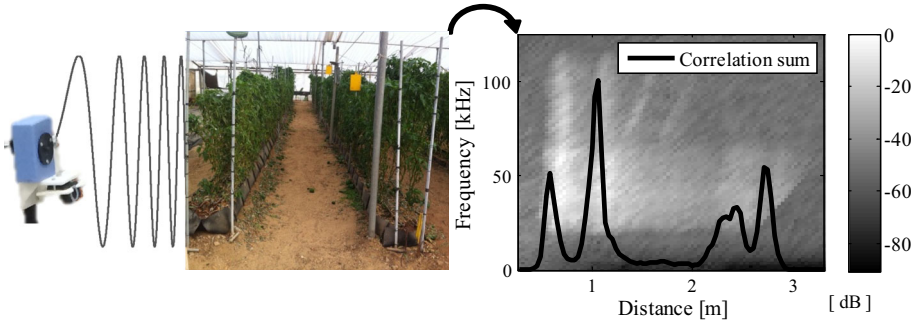


**Fig. 5** **a** Side view of two pepper plant rows. **b** Mean spectrogram and 40–60 kHz correlation sum

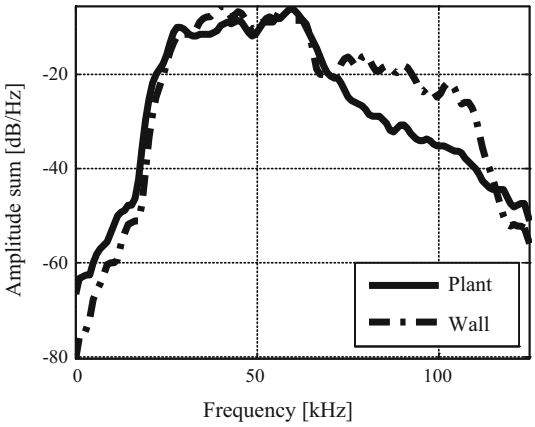


**Fig. 6** Wall and plant spectrum at 1.0 m

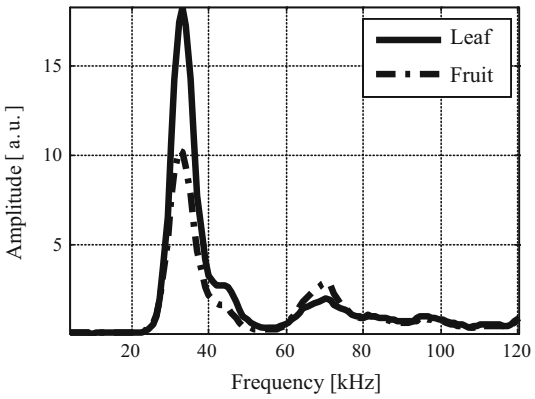


**Fig. 7** Frequency spectrum of leaves and fruit. Amplitude is normalized. Units are arbitrary and normalized per frequency by the maximum input amplitude

harmonic at 70 kHz is higher than the leaves. This could be explained by the increasing directivity of acoustic speakers with frequency. The increasing directivity could be the reason that the effects of area orthogonal to the ultrasonic sensor is due to other acoustic phenomenon. While the absolute standard deviation at 33 and 70 kHz for a single fruit was 8.6 and 3.4 respectively, for leaves, the standard deviation was 17 and 1.5. This difference in variance in the lower frequencies can be explained by the spherical axisymmetric shape of the fruit which cancels the influence of orientation in relation to leaves that return almost nothing when they are not perpendicular.

## Lab experiment

In this experiment, five plants were tested at three orientations (total of 15 $P_iO_j$) from distances of 1.25 and 0.625 m. Each trial was ensonified 30 times each, with different amounts of fruit. The mean spectrogram of the echoes of the 30 ensonfications for each $P_iO_j$ was normalized by the CHIRP intensity of each frequency (as described in the "Data acquisition and basic signal processing" section above) forming a normalized echo spectrogram. The mean echo spectrogram of the post harvest plants $P_iO_j$ were subtracted from the spectrogram of a pre-harvest plants $P_iO_j$ to highlight the differences in the echoes

of the specific plant and specific orientation $\left(P_i O_j\right)$ with different amount of fruits, e.g. Fig. 8c = Fig. 8a – Fig. 8b. Figure 8 demonstrates this relationship for $P_1 O_1$.

Positive differences between the spectrograms represent frequency–distance areas in which the unpicked plant returns higher amplitudes than the plant with no fruits and vice versa. To avoid a situation in which these differences are balancing each other, the positive and negative differences were summed separately for each frequency. The sums of the positive differences for each $P_i O_j$ are displayed in Fig. 9.

The local maximum values of each plant and orientation in Fig. 9 express special frequencies of interest that conceal more information about the difference between empty and unpicked plants. Figure 10 illustrates the superposition of a number of local maxima at a resolution of 0.488 kHz for all $P_i O_j$.

The number of peaks for frequencies 20, 33, 68, 96 and 116 kHz is over 10 (out of possible maximum 15) which stands out in their neighborhood ($\pm 10$) kHz. For this reason, these frequencies neighborhood were considered more carefully when specifying frequency bands for the statistical analysis. A multi-linear regression estimating the energy level $E^{ij}$ was computed as described in the "Materials and methods" section in frequencies range of 28–32 kHz in 10 800 observations. The results are displayed in Table 2 which unveils a high level of significance as the null hypothesis is rejected for all variables with high probability (P-value under 0.001) and the adjusted $R^2$ indicates that the model explains 64% of the variance in the data set. The energy–mass relation was monotonic and descending; this means that the existence of fruit attenuates the echoes from the plants in accordance with the single fruit and leaves experiment that showed that fruit return lower amplitudes.

The indicator variables, $\delta^{ij}$, vary between $-2.61 \times 10^{-8}$ and $2.99 \times 10^{-8}$ $\mathrm{WHz}^{-1}$ with high levels of significance ($P \ll 0.001$). This suggests that the influence of the geometry of the single plant cannot be ignored and therefore an estimation of the mass is not possible at these frequencies without bypassing the indicator variables problem (see Eq. 5) Fig. 11 shows the fitness level of the energy predicted by the model to the energy measured in the lab experiment for each plant and orientation.

Figure 11 shows that most of the plant-orientation combinations lie around the 45° line representing complete fitness between the predicted and the measured energy.

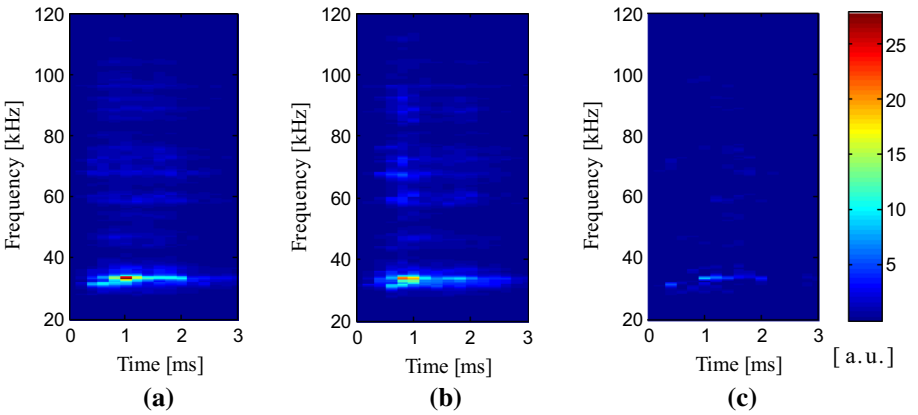


**Fig. 8** **a** Mean normalized echo for unpicked $P_1 O_1$ **b** Mean normalized echo for empty $P_1 O_1$ **c** Difference between $P_1 O_1$ normalized mean echoes

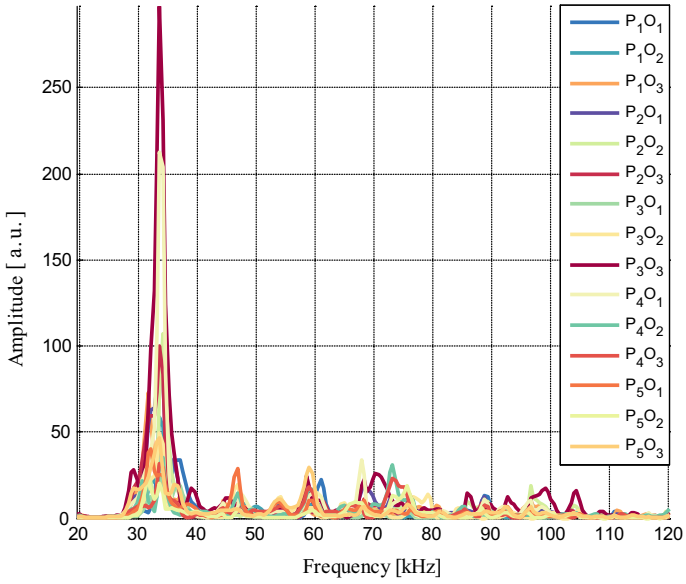


**Fig. 9** Sum of positive changes between spectrograms. The amplitude is normalized per frequency

**Fig. 10** The number of peaks per frequency for the 15 plant-orientation combinations

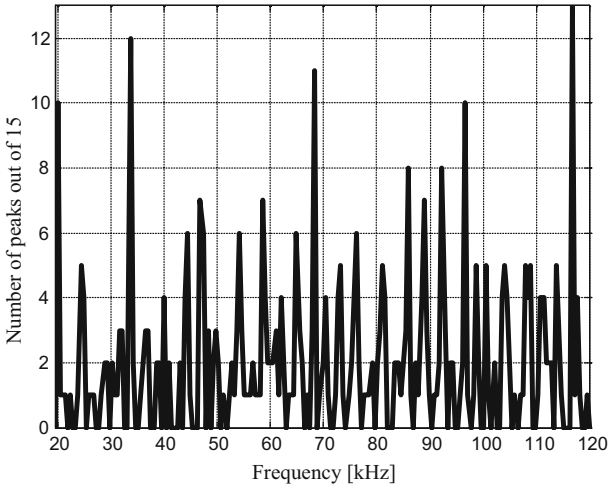


**Table 2** Summary of the regression parameters when estimating the model in Eq. (3) in the range 28–32 kHz

| Variable | Estimate | Standard error | T-Statistics | P |
|---|---|---|---|---|
| $f^{ij}$ | 3.32E−12 | 1.68E−13 | 19.752 | 2.46E−85 |
| $m^{ij}$ | −7.79E−11 | 9.39E−12 | −8.2996 | 1.17E−16 |
| $m^{ij}f^{ij}$ | 1.55E−15 | 3.11E−16 | 4.9827 | 6.37E−07 |
| $m^{ij2}$ | −1.57E−16 | 5.48E−18 | −28.684 | 1.96E−174 |
| $f^{ij2}$ | 2.71E−14 | 8.90E−16 | 30.444 | 2.30E−195 |

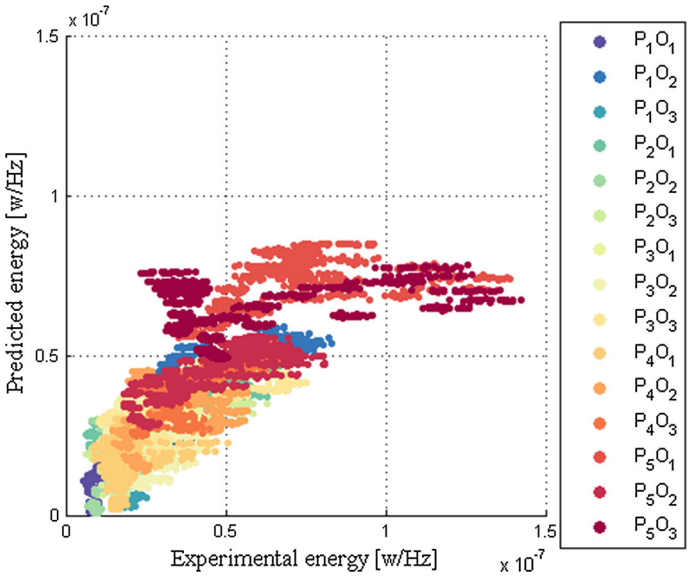


**Fig. 11** Predicted against experimental results for frequencies of 28–32 kHz

A similar analysis on 22 950 observations at 20–28 kHz using a quadratic model that does not include indicator variables individual to each $P_iO_j$ revealed that the calculated multi-linear regression values (Table 3) maintain their high level of significance in rejecting the null hypothesis, adjusted $R^2$ of 0.839 and a P-value under 0.001. The energy–mass relation was also monotonic and descending with a highly linear influence.

These high levels of significance without using the indicator variables in the model allowed the extraction of the mass to frequencies and energy returns relation in Eq. (5) without the noisy outcome of numerical differentiation necessary in Eq. (6).

Figure 12 shows the fitness level of the energy predicted by the model to the energy measured in the lab experiment for each plant and orientation.

To overcome noise and improve the results, the sampled energy was filtered at each frequency by a median filter before the prediction. The filtered data is used together with Eq. (5) to obtain an estimation of the mass displayed in Fig. 13. The results are averaged for each plant #*i* from all three orientations for each plant mass level.

The linear relationship between predicted and experimental mass is shown in Fig. 13 and has an $R^2$ of 0.34. The estimation accuracy can be improved by acquiring more samples of the plants from different orientations. Obtaining data from several orientations

**Table 3** Summary of the regression parameters when estimating a quadratic model in the range 20–28 kHz

| Variable | Estimate | Standard Error | T-Statistic | P |
|---|---|---|---|---|
| 1 | 8.32E−08 | 1.61E−09 | 51.526 | 0 |
| $f^{ij}$ | −8.14E−12 | 1.35E−13 | −60.108 | 0 |
| $m^{ij}$ | −1.24E−11 | 4.06E−13 | −30.553 | 5.49E−201 |
| $m^{ij}f^{ij}$ | 5.90E−16 | 1.64E−17 | 35.961 | 1.49E−275 |
| $m^{ij2}$ | 2.03E−16 | 2.82E−18 | 72.034 | 0 |
| $f^{ij2}$ | −4.47E−16 | 8.71E−17 | −5.1254 | 2.99E−07 |

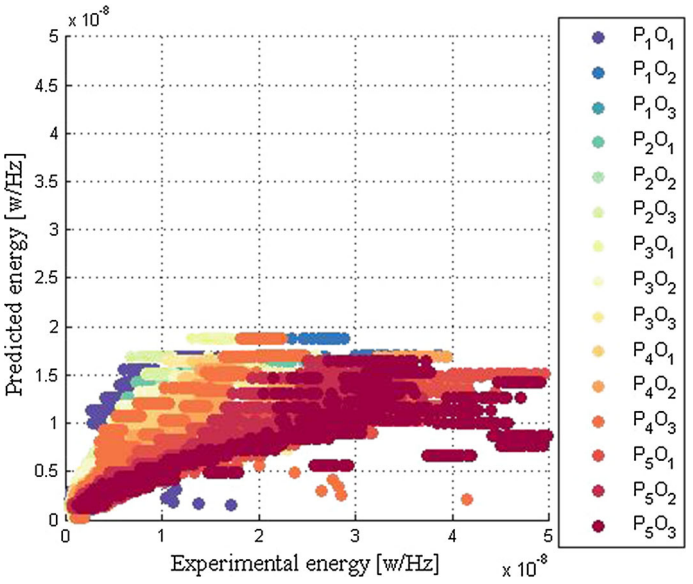


**Fig. 12** Predicted against experimental results for frequencies of 20–28 kHz

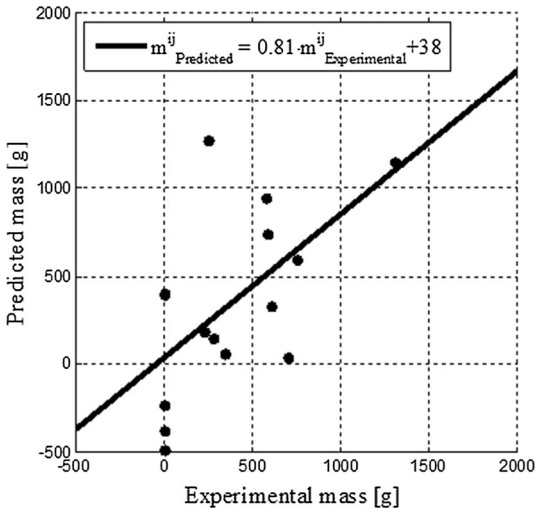


**Fig. 13** Predicted against experimental mass

can be a rigorous task well suited for a robot as intended and already used by the authors. Moreover, the full potential of the information residing in the spectrum needs to be investigated further using additional frequency bands as seen in Fig. 10 that have not been used thus far.

## Conclusions

An ultrasonic system for yield assessment and greenhouse features identification was developed and tested in lab and greenhouse environments.

The developed system can detect and map crop rows without a direct line of sight using a matched filter and normalizing the acoustic energy by distance.

The spectrum signature of walls and screens (greenhouse infrastructures) can be characterized and distinguished from the greenhouse vegetation at high ultrasonic frequencies. These differences have been implemented to discriminate between walls and plants.

Single fruits were found to return less energy than leaves at low frequencies because of their shape, expressed by a small surface perpendicular to the sensing system. At 30 kHz single leaves return more energy than in other frequencies and more than in fruit.

A multi-linear regression model for estimating the energy level was found to be highly significant and correlated in the range 20–33 kHz range. An echo to mass model was developed. The results indicate that pepper fruit mass on the plants are correlated with energy and frequency at a number of frequency bands. The relation between fruit mass and energy returning from the plant was in general monotonic and decreasing.

Using more frequency bands, ensonifying the plants from several directions, obtaining more samples from each plant and increasing the amplitude of the emitted signals will improve the estimations of the mass and energy evaluation models.

**Acknowledgements** Special thanks to Raimund Specht from Avisoft for the technical help with the ultrasonic equipment, Yossi Kamir for the help in 3D printing the sensor system enclosures and to Yossi Portal for the dedicated nurturing of the greenhouse and plants.

## References

Akbarally, H., & Kleeman, L. (1995). A sonar sensor for accurate 3D target localisation and classification. In: *IEEE International Conference on Robotics and Automation, Proceedings.,* (Vol. 3, pp. 3003–3008). doi:10.1109/ROBOT.1995.525710.

Andújar, D., Escola, A., Dorado, J., & Fernandez-Quintanilla, C. (2011). Weed discrimination using ultrasonic sensors. *Weed Research, 51*(6), 543–547. doi:10.1111/j.1365-3180.2011.00876.x.

Andújar, D., Fernández-Quintanilla, C., & Dorado, J. (2015). Matching the best viewing angle in depth cameras for biomass estimation based on poplar seedling geometry. *Sensors, 15*(6), 12999–13011.

Balleri, A., Griffiths, H. D., Baker, C. J., Woodbridge, K., & Holderied, M. W. (2012). Analysis of acoustic echoes from a bat-pollinated plant species: Insight into strategies for radar and sonar target classification. *IET Radar, Sonar and Navigation, 6*(6), 536–544. doi:10.1049/iet-rsn.2011.0259.

Bloch, V., Degani, A., & Bechar, A. (2015). Task characterization and classification for robotic manipulator optimal design in precision agriculture. In: Stafford, J. V. (Ed.) *Precision Agriculture '15, Proceedings of the 10th European Conference on Precision Agriculture* (pp. 313–320). Wageningen, The Netherlands: Wageningen Academic Publishers.

Finkelshtain, R., Yovel, Y., Kosa, G., & Bechar, A. (2015). Detection of plant and greenhouse features using sonar sensors. In Stafford, J. V. (Ed.) *Precision Agriculture '15, Proceedings of the 10th European Conference on Precision Agriculture* (pp. 299–306). Wageningen, The Netherlands: Wageningen Academic Publishers.

Harper, N., & McKerrow, P. (2001). Recognising plants with ultrasonic sensing for mobile robot navigation. *Robotics and Autonomous Systems, 34*(2–3), 71–82. doi:10.1016/S0921-8890(00)00112-3.

Kleeman, L., & Kuc, R. (2008). Sonar Sensing. In B. Siciliano & O. Khatib (Eds.), *Springer handbook of robotics* (pp. 491–519). Berlin, Germany: Springer.

Lee, W., Alchanatis, V., Yang, C., Hirafuji, M., Moshou, D., & Li, C. (2010). Sensing technologies for precision specialty crop production. *Computers and Electronics in Agriculture, 74*(1), 2–33.

Lim, Z., Kwon, S., & Joo, M. (2012). Multi-object identification for mobile robot using ultrasonic sensors. *International Journal of Control, Automation and Systems, 10*(3), 589–593. doi:10.1007/s12555-012-0316-6.

McKerrow, P., & Harper, N. (1999). Recognising leafy plants with in-air sonar. *Sensor Review, 19*(3), 202–206. doi:10.1108/02602289910279139.

McKerrow, P. J., & Kristiansen, B. E. (2006). Classifying surface roughness with CTFM ultrasonic sensing. *IEEE Sensors Journal, 6*(5), 1267–1279. doi:10.1109/JSEN.2006.881419.

Mizrach, A. (2008). Ultrasonic technology for quality evaluation of fresh fruit and vegetables in pre-and postharvest processes. *Postharvest Biology and Technology, 48*(3), 315–330.

Mizrach, A., Bechar, A., Grinshpon, Y., Hofman, A., Egozi, H., & Rosenfeld, L. (2003). Ultrasonic mealiness classification of apples. *Transactions of the ASAE, 46*(2), 300–397.

Moonrinta, J., Chaivivatrakul, S., Dailey, M. N., & Ekpanyapong, M. (2010). Fruit detection, tracking, and 3D reconstruction for crop mapping and yield estimation. In *Proceedings of the International Conference on Intelligent Robots and Systems* (pp. 1181–1186). Singapore: IEEE.

Müller, R., & Kuc, R. (2000). Foliage echoes: A probe into the ecological acoustics of bat echolocation. *The Journal of the Acoustical Society of America, 108*(2), 836–845.

Müller, S., & Massarani, P. (2001). Transfer-function measurement with sweeps. *Journal of the Audio Engineering Society, 49*(6), 443–471.

Nuske, S., Achar, S., Bates, T., Narasimhan, S., & Singh, S. 2011. Yield estimation in vineyards by visual grape detection. In *IEEE/RSJ International Conference on Intelligent Robots and Systems* (*IROS*), (pp. 2352–2358). doi:10.1109/IROS.2011.6095069.

Ping, H. (1998). Simulation of ultrasound pulse propagation in lossy media obeying a frequency power law. *IEEE Transactions on Ultrasonics, Ferroelectrics, and Frequency Control, 45*(1), 114–125. doi:10.1109/58.646916.

Stajnko, D., Lakota, M., & Hočevar, M. (2004). Estimation of number and diameter of apple fruits in an orchard during the growing season by thermal imaging. *Computers and Electronics in Agriculture, 42*(1), 31–42.

Steckel, J., & Peremans, H. (2013). BatSLAM: Simultaneous localization and mapping using biomimetic sonar. *PLoS ONE, 8*(1), e54076. doi:10.1371/journal.pone.0054076.

Toda, M., Kitani, O., Okamoto, T., & Torii, T. (1999). Navigation method for a mobile robot via sonar-based crop row mapping and fuzzy logic control. *Journal of Agricultural Engineering Research, 72*(4), 299–309.

Wachs, J. P., Stern, H. I., Burks, T., & Alchanatis, V. (2010). Low and high-level visual feature-based apple detection from multi-modal images. *Precision Agriculture, 11*(6), 717–735. doi:10.1007/s11119-010-9198-x.

Yovel, Y., Franz, M. O., Stilz, P., & Schnitzler, H.-U. (2008). Plant classification from bat-like echo location signals. *PLoS Computational Biology, 4*(3), e1000032. doi:10.1371/journal.pcbi.1000032.

Yovel, Y., Stilz, P., Franz, M. O., Boonman, A., & Schnitzler, H.-U. (2009). What a plant sounds like: The statistics of vegetation echoes as received by echo locating bats. *PLoS Computational Biology, 5*(7), e1000429. doi:10.1371/journal.pcbi.1000429.